Associative Mechanism for Phosphoryl Transfer: A Molecular Dynamics Simulation of *Escherichia coli* Adenylate Kinase Complexed With Its Substrates

Harini Krishnamurthy,[1,2,4] Hongfeng Lou,[3,4] Adam Kimple,[3,4] Claire Vieille,[1] and Robert I. Cukier[3,4]*
[1]*Department of Biochemistry and Molecular Biology, Michigan State University, East Lansing, Michigan*
[2]*Graduate Program in Cell and Molecular Biology, Michigan State University, East Lansing, Michigan*
[3]*Department of Chemistry, Michigan State University, East Lansing, Michigan*
[4]*MSU Center for Biological Modeling, Michigan State University, East Lansing, Michigan*

ABSTRACT **The ternary complex of *Escherichia coli* adenylate kinase (ECAK) with its substrates adenosine monophosphate (AMP) and Mg-ATP, which catalyzes the reversible transfer of a phosphoryl group between adenosine triphosphate (ATP) and AMP, was studied using molecular dynamics. The starting structure for the simulation was assembled from the crystal structures of ECAK complexed with the bisubstrate analog diadenosine pentaphosphate (AP_5A) and of *Bacillus stearothermophilus* adenylate kinase complexed with AP_5A, Mg^{2+}, and 4 coordinated water molecules, and by deleting 1 phosphate group from AP_5A. The interactions of ECAK residues with the various moieties of ATP and AMP were compared to those inferred from NMR, X-ray crystallography, site-directed mutagenesis, and enzyme kinetic studies. The simulation supports the hypothesis that hydrogen bonds between AMP's adenine and the protein are at the origin of the high nucleoside monophosphate (NMP) specificity of AK. The ATP adenine and ribose moieties are only loosely bound to the protein, while the ATP phosphates are strongly bound to surrounding residues. The coordination sphere of Mg^{2+}, consisting of 4 waters and oxygens of the ATP β- and γ-phosphates, stays approximately octahedral during the simulation. The important role of the conserved Lys13 in the P loop in stabilizing the active site by bridging the ATP and AMP phosphates is evident. The influence of Mg^{2+}, of its coordination waters, and of surrounding charged residues in maintaining the geometry and distances of the AMP α-phosphate and ATP β- and γ-phosphates is sufficient to support an associative reaction mechanism for phosphoryl transfer. Proteins 2005;58:88–100.**

Key words: adenylate kinase; ATP and AMP; molecular dynamics; phosphoryl transfer

INTRODUCTION

Adenylate kinases (AKs) are small, monomeric phosphoryl transferases that catalyze the reversible transfer of a phosphoryl group from adenosine triphosphate (ATP) to adenosine monophosphate (AMP) by nucleophilic attack on the γ-phosphate of ATP.[1] The net reaction is schematized as

$$Mg^{2+}\text{-ATP} + \text{AMP} \Leftrightarrow Mg^{2+}\text{-ADP} + \text{ADP} \quad \text{(Scheme 1)}$$

AKs are composed of 3 domains: the core, LID, and AMP-binding (AMP-bd) domains (Fig. 1). In the absence of substrates, AKs are in an open form. In the presence of ATP, AMP, and Mg^{2+}, the LID and AMP-bd undergo major conformational rearrangements, resulting in the enzyme closing to form the ternary complex and expelling waters to prevent ATP and AMP hydrolysis.[2] The best-known AK families are the short AKs represented by the mammalian cytosolic enzymes, and the long AKs represented by bacterial and mitochondrial enzymes. The long AKs contain a 20- to 30-residue insertion inside the LID domain.[3,4] Among the short AKs, only the porcine cytosolic AK has been crystallized in the absence of substrate [Protein Data Bank (PDB) code: 3ADK).[5] On the other hand, the long AKs from *Escherichia coli* (ECAK), *Bacillus stearothermophilus*, *Saccharomyces cerevisiae,* and bovine mitochondria have been crystallized with various substrate–inhibitor combinations or with the 5-phosphate bisubstrate analog, diadenosine pentaphosphate (i.e., AP_5A).[6–15] The crystal structures of the *E. coli* and bovine mitochondrial AKs in the absence of any ligands are also known.[10,16] ATP binds to the catalytic site as the Mg^{2+}-ATP complex, in which the catalytically essential Mg^{2+} is coordinated to ATP's β- and γ-phosphates and to 4 water molecules. Thus, the functional catalytic assembly is a ternary complex. In this work, we focus on ECAK, since a wealth of kinetic,[17] NMR,[18–22] and mutagenesis[23–28] data are available for this enzyme.

Crystallography can provide structures of enzymes complexed with products, with inhibitors that resemble sub-

Grant sponsor: USDA; Grant number: 2003-34189-13421. Grant sponsor: NIH; Grant number: GM62790. Grant sponsor: MSU Center for Biological Modeling (fellowships to H. Krishnamurthy, H. Lou, and A. Kimple).

*Correspondence to: R. I. Cukier, Dept. of Chemistry, Michigan State University, East Lansing, MI 48224-1322. E-mail: cukier@cem.msu.edu

Received 7 April 2004; Accepted 13 July 2004

Published online 1 November 2004 in Wiley InterScience (www.interscience.wiley.com). DOI: 10.1002/prot.20301

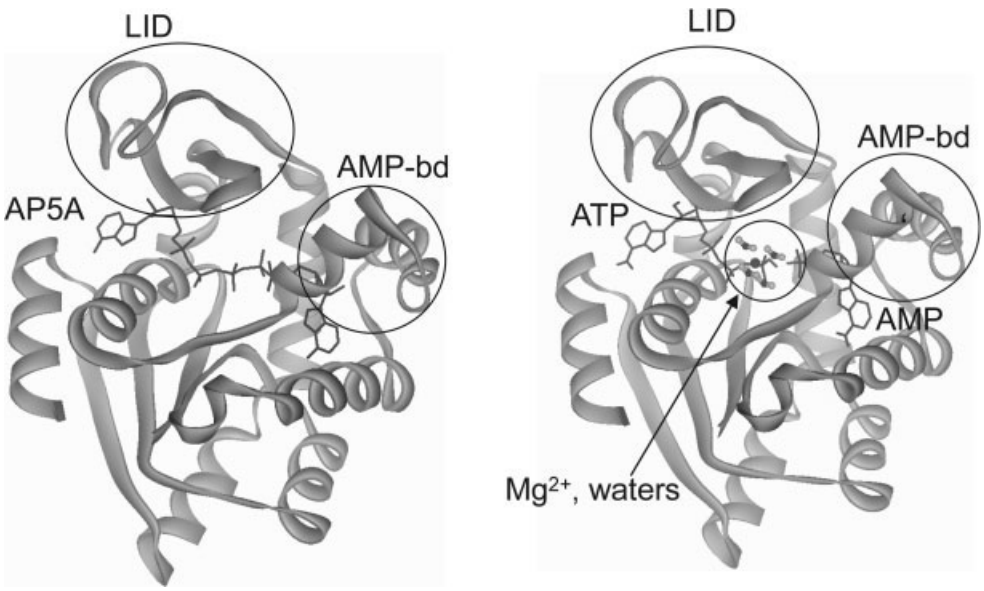

Fig. 1. Structures of 1AKE (**left**) and 1AKE* (**right**). ECAK is show in ribbon representation. AP_5A, ATP, and AMP are in stick representation; the Mg^{2+} atom and its 4 coordinating waters are in ball-and-stick representation. ATP and AMP were created by deleting AP_5A's δ-PO_4. Mg^{2+} and its coordinating waters were imported from the 1ZIO structure.

strates, and even with inhibitors that model transition states. In this work, we create a model of the ECAK · Mg-ATP · AMP ternary reaction complex based on the ECAK · AP_5A structure (PDB code: 1AKE)[6] and on the *B. stearothermophilus* AK (BSAK) structure crystallized with AP_5A and Mg^{2+} (PDB code: 1ZIO).[11] Constructing a reaction complex model allows one to study the stabilization of a possible catalytically competent complex that is more realistic than a model inferred from a crystal structure containing substrate mimics. Thus, the ternary complex model will be used as the starting point of a molecular dynamics (MD) simulation that can assess how ATP and AMP are maintained in a catalytically competent configuration with the aid of the surrounding protein, the Mg^{2+} ion, and its 4 coordinating waters. The highly charged complex suggests a focus on strong hydrogen bonds (H-bonds) and salt bridges that can serve the purpose of maintaining a catalytically relevant geometry.

Two simulations of AKE have appeared previously. One, a 300-ps study of ECAK complexed with AP_5A, was carried out in the gas and solvated states.[29] A number of residues that would be candidates for strong interaction with a Mg^{2+} ion were suggested in this study. The other simulation used a weighted masses MD method to explore the nature of the open conformation of apo-ECAK that could be reached starting from a number of closed form (with different bound substrates) crystallographic structures.[30]

The similarities and differences between various experimental conclusions based mainly on studies using AP_5A, and the simulation of the ECAK · Mg-ATP · AMP structure are analyzed. While there are some differences in details, the suggested distinction between the high specificity of AKs for the AMP substrate and the lower specificity for ATP is supported by the simulation. Particular attention is devoted to investigating the interactions of the conserved Lys13 (the numbering refers to ECAK) located at the end of the P loop, with the AMP and ATP phosphate groups. The simulation shows that Lys13 does play an important role in substrate stabilization by bridging the AMP and ATP phosphates.

There is great interest, in general, in the mechanism of phosphoryl transfers, whether it is an associative or a dissociative mechanism, these being extremes of a continuum of mechanisms qualitatively defined by the phosphorous–phosphorous distance, which increases in going from an associative to a dissociative mechanism.[25,31–34] There is evidence[32] that a dissociative mechanism is favored in solution, while an associative mechanism is favored in enzymes. The nature of the transition state (or reaction intermediate) also is an issue, with the most frequently suggested geometry invoking a pentavalent phosphorous.[25,31–34] As we discuss, the simulation carried out herein maintains the AMP and ATP terminal phosphates at a distance that supports an associative phosphoryl transfer mechanism.

METHODS

Starting Structure

The 1.9 Å resolution crystal structure of the ECAK · Ap_5A complex[7] (PDB code: 1AKE) was used as the starting point for constructing an ECAK · AMP · Mg^{2+}-ATP ternary complex, which will be denoted as 1AKE*. The 1AKE PDB file contains the coordinates of the 2 enzyme–inhibitor complexes (A and B) present in the crystal asymmetric unit. We used complex B to build 1AKE*. AP_5A (Fig. 1) is considered to be a bisubstrate mimic of the reactant state, since ECAK catalyzes the reaction of ATP and AMP to produce two ADPs (Scheme 1). ATP and AMP coordinates

were obtained by eliminating AP_5A's δ-PO_4 group (see Fig. 1).

While the 1AKE structure provides the AP_5A coordinates needed to create well-positioned ATP and AMP molecules within the protein, it does not contain the catalytic Mg^{2+} and its 4 waters of coordination. To create the starting structure for the MD simulation, we imported the coordinates of Mg^{2+} and its coordinated waters from the crystal structure of the BSAK · Mg^{2+}-AP_5A complex (PDB code: 1ZIO).[11] The 1ZIO and 1AKE structures were superimposed by fitting 1ZIO's AP_5A molecule onto that of 1AKE. 1ZIO's Mg^{2+} and its 4 coordination waters were then merged with the ECAK · AMP · ATP structure to create 1AKE*. This structure contains Mg^{2+} positioned between nonbridging oxygens of ATP's β-and γ-phosphates and the 4 Mg^{2+} coordinating waters, as displayed in Figure 1.

Force Field

The GROMOS96 force-field was used for the MD simulations.[35] This force field is a united atom force field with explicit polar hydrogens, and hydrogens on the phenylalanine, tryptophan, and tyrosine rings. The GROMOS96 force field contains parameters for all protein residues, as well as for ATP, but it does not include parameters for AMP. Parameters for AMP were created based on the ATP parameters.[35] The force field is identical up to atom 23 (A05* as numbered on ATP). The parameters from 32 (APG) to 36 (AH3PG) in ATP are then used for AMP's monophosphate group.

The ionization states of all residues were set to reflect a neutral pH. Histidines were assumed to be neutral, with the Nδ atom protonated, and the lysine, arginine, aspartate, and glutamate residues were assumed to be charged. To assess whether this charge assignment is reasonable in the binding pocket, where numerous positively charged residues bind the substrate phosphates, we adopted the following procedure. The accessible surface area (ASA) of each residue was evaluated using the Surface Racer program,[36] for the residues in the 1AKE* complex and in the 1AKE* structure in the absence of the substrates. For each residue, the ASA in the presence of substrate was subtracted from the ASA in the absence of substrate. The nonzero ASA difference values then single out those residues that are buried at the protein–substrate interface. The charged residues buried at the protein–substrate interface, Lys13, Arg36, Asp84, Arg88, Arg119, Arg123, Arg156, and Asp158, have a net charge of +4. These charges are almost compensated, through various interactions discussed below, by the net charge of −2 from ATP (−3, with 1 terminal oxygen protonated), AMP (−1), and Mg^{2+} (+2). A look at the charged residues buried at the protein–substrate interface shows that, with the exception of Arg123, all the ionizable groups on positively charged residues are engaged in charge–charge interactions with the substrate phosphates. All these charge–charge interactions are stable throughout the 3-ns simulation period (see below). The side-chain of Asp84 is engaged in stable H-bonds with 2 of the waters coordinated to Mg^{2+}, namely, 219 and 221. Arg123 forms a salt bridge with Asp159, which is also stable during the simulation. Note that Asp159, along with its neighboring Asp158 at the C-terminal end of the LID domain, are conserved in all AKs implicating a crucial role for them in AKs. These 2 aspartates form salt bridges with Arg123 and Arg156 side-chains only in the substrate bound form. Müller and Schulz[7] suggested that salt bridges Arg123–Asp159 and Arg156–Asp158 (formed with the aid of ATP and AMP, which help in positioning the side-chains) are instrumental in the conformational change leading to LID closure. Thus, the conventional ionization states assumed in this study are appropriate, since almost all of the charged groups buried in the 1AKE* complex have their charges satisfied either through protein–substrate, or protein–protein interactions.

Molecular Dynamics

The MD simulation was carried out using CUKMODY,[37] a code designed for the efficient simulation of proteins and other large solutes. A combination of a cell index method with linked lists[38] and a Verlet neighbor list[39] is used to provide linear scaling with the number of atoms in the pair list routine, essential for the large systems considered here. For the Verlet neighbor list, the outer distance was r_l = 11.84 Å and the inner distance was r_c = 10.42 Å. The pair list was updated whenever any atom moved a distance greater than $0.5*(r_l - r_c)$, leading to updates roughly every 25 steps. Electrostatic interactions are evaluated using the charge-group method, to be consistent with the parametrization of the GROMOS force field. The SHAKE algorithm[39] was used to constrain bond lengths permitting a 2-fs timestep. Periodic boundary conditions were used. The simulation was carried out at constant number, volume, and temperature (NVT), with velocity scaling to control the temperature at 303 K. The runs were all performed on a PC with dual 1.6GHz AMD Athlon processors. A 1-ns simulation takes about 2 weeks on a single processor.

Equilibration

The 1AKE* system was equilibrated according to the following protocol. A simulation box of side 59.19 Å was filled with an equilibrated sample of 6912 waters, and the 1AKE* structure, totaling 2162 atoms, was centered in the simulation cell. The waters that overlapped any 1AKE* atom were discarded if $r_{Oj} < \sigma_{Oj}$, where r_{Oj} is the distance between water oxygen (atom O) and protein atom (atom j), and σ_{Oj} is the van der Waals distance parameter. This procedure eliminated 1470 waters. One-body forces, with force constant k = 30 kcal/mol/Å^2, were used on all protein and ligand atoms for the initial 50,000 steps. This procedure allowed the waters to equilibrate with the protein and with each other. The van der Waals length (σ) and well depth (ε) values for the water oxygen–Mg^{2+} interactions were designed to maintain coordination throughout the simulations. To enforce the initial water coordination of Mg^{2+}, the parameters listed in Table I were used to equilibrate the system and then modified as indicated for the duration of the simulation.

TABLE I. Water-Mg^{2+} Van der Waals Parameters for the Mg^{2+} Coordination Waters During the MD Equilibration and Simulation Periods

	Equilibrate with		Run with	
	σ^a (Å)	ε^a (K)	^{a} (Å)	ε^a (K)
Water 218	2.16137	50,000.0	2.07364	54,273.3
Water 219	2.07814	20,000.0	2.07364	54,273.3
Water 220	1.88086	20,000.0	2.07364	54,273.3
Water 221	2.19517	50,000.0	2.07364	54,273.3

[a]The van der Waals interaction between atoms i and j is $V = 4\varepsilon_{ij}[(r_{ij}/\sigma_{ij})^{12} - (r_{ij}/\sigma_{ij})^6]$, where $\sigma_{ij} = (\sigma_i + \sigma_j)/2$ and $\varepsilon_{ij} = \sqrt{\varepsilon_i \varepsilon_j}$.

After the initial 50,000 steps with one-body forces on, the one-body force constant was linearly reduced to 0 over 30,000 steps. The system was then run for another 20,000 steps to make sure that the system's strain was sufficiently reduced to initiate unconstrained dynamics. A 0.5-ns trajectory was run at 273 K, after which the temperature was linearly brought to 303 K over 10,000 steps. After the temperature had reached 303 K, the MD production trajectory proceeded for 3 ns.

H-bond–Salt Bridge Analysis

Interactions of AMP and ATP with 1AKE* residues were analyzed through H-bond analysis. Donor and acceptor atoms within a maximum distance of 3.5 Å and a minimum angle of 120° were considered to form H-bonds. The data were analyzed every 0.8 ps. Interactions between a charged phosphate group of the substrates and the side-chain of a positively charged residue (arginine or lysine) were considered to be salt bridge–like. Oppositely charged groups within 4.5 Å of each other were considered to be salt-bridged.

RESULTS AND DISCUSSION

Validation of Simulation

The radius of gyration of the protein increases very slowly during the first 740 ps, with an average of 17.18 ± 0.09 Å during that period and, subsequently, suddenly increases and stabilizes to an average of 17.60 ± 0.11 Å during the remainder of the simulation, indicating that the overall dimension of the protein is stable. (The radius of gyration of 1AKE in the crystal structure is 16.635 Å.)

The RMSD (i.e., root-mean-square deviation from the starting 1AKE* structure) for all Cα's increases slowly from 1.5 to 3.1 Å during the first 800 ps of the production trajectory; then, between 1100 and 1300 ps, it increases more sharply to finally plateau between 4.0 and 5.0 Å during the rest of the simulation. The RMSD for the Cα's of the core domain (residues 1–30, 60–120, and 160–214) increases very slowly to 2.3 Å during the first 1 ns of the production trajectory, then plateaus between 2.1 and 2.75 Å before finally increasing after 2800 ps. The RMSD for the Cα's of the core plus the AMP-bd domains (residues 1–120 and 160–214) increases during the first 800 ps at the same rate as the RMSD for all Cα's, then oscillates between 2.5 and 3.4 Å during the next 2000 ps, before finally increasing after 2800 ps. These results indicate that the deviation from the crystal structure is not distributed uniformly along the sequence, and that most of the large deviations (in particular after the first 1200 ps) occur in the LID domain.

To compare residue fluctuations in 1AKE* with those in the 1AKE crystal, RMSF values (i.e., positional root-mean-square fluctuations from the average structure) were calculated for all Cα carbons as $\mathrm{RMSF}_n = \langle(r_n - \langle r_n\rangle)^2\rangle^{\frac{1}{2}}$, with $\langle r_n\rangle$ being the average position of the Cα carbon of residue n over time, and r_n being the position at every step. Simulation RMSF values are compared with 1AKE crystallographic RMSF values in Figure 2. Crystallographic RMSF values were calculated from the B values using the equation $\mathrm{RMSF} = \sqrt{3B/8\pi^2}$. Regions with low RMSF values (e.g., helices α_4 and α_8, and strand β_4) in the simulation coincide well with the regions with low crystallographic RMSF values. In contrast, the regions showing high simulation RMSF values and high crystallographic RMSF values do not always match each other. Residues 41–48 (the loop between helices α_2 and α_3), and 132–140 (the loop between strands βL_2 and βL_3) show high simulation RMSF values that were not expected from their average crystallographic RMSF values. Residues 74–79 (the loop between helix α_4 and strand β_3) show the opposite trend: Although they have the highest crystallographic RMSF values in 1AKE (1.72 ± 0.17 Å for 74–79 Cα's against an average B factor of 1.001 ± 0.19 Å for all Cα's), these residues show simulation RMSF values (2.16 ± 0.49 Å) only slightly above the average for the protein (1.93 ± 0.94 Å).

The low crystallographic RMSF values associated with residues 42–48 in 1AKE might be due to the fact that residues 44, 45, 47, and 48 are involved in crystal contacts.[7] In the simulation, the absence of crystal contacts results in a larger conformational freedom for this region of the protein. In this respect, it is interesting to note that residues 46–48 adopt different secondary structures in 1AKE complexes I and II.[7] Müller et al.[10] later noticed that residues 44–48 are part of helix α3 in the apo-enzyme (PDB code: 4AKE). These crystallographic observations suggest that this region is highly susceptible to conformational changes, and they agree with the large RMSF values observed for residues 41–48 in our simulation.

Because residues 74–79 have the highest crystallographic RMSF values in 1AKE, and because these residues have lower crystallographic RMSF values in the apo-enzyme, it was suggested that this loop is part of an energy counterweight in ECAK.[10] The low RMSF values observed for residues 74–79 in our simulation do not support this energy counterweight hypothesis. Another possibility is that the high crystallographic RMSF values of residues 74–79 are an artifact of crystallization. In 1AKE, this loop is involved in crystal contacts: Glu75 forms a H-bond and salt bridge with Asp76 and Arg78 of another molecule, respectively.[7] These interactions might force this loop into a conformation that is not 100% occupied or that would not be favored in solution. Some of these differences may be attributable not only to the different conditions involved in crystalline versus liquid

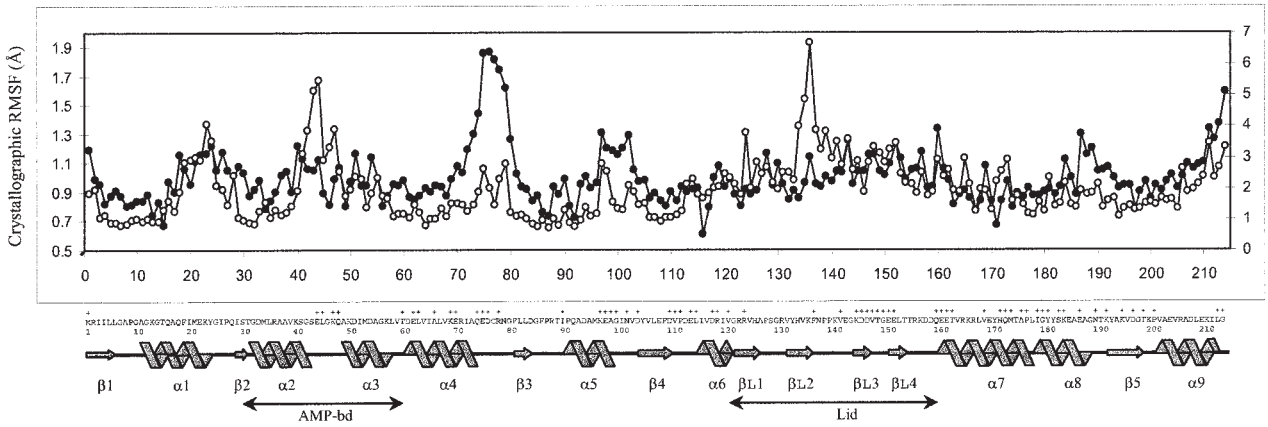

Fig. 2. Comparison of 1AKE crystallographic (●) and simulation RMSF values (○) for all Cα atoms. Residues involved in crystal contacts (+ signs) are indicated at the bottom of the graph. Secondary structure elements are shown as published.[7] AMP-bd and LID domains are indicated by two-headed arrows.

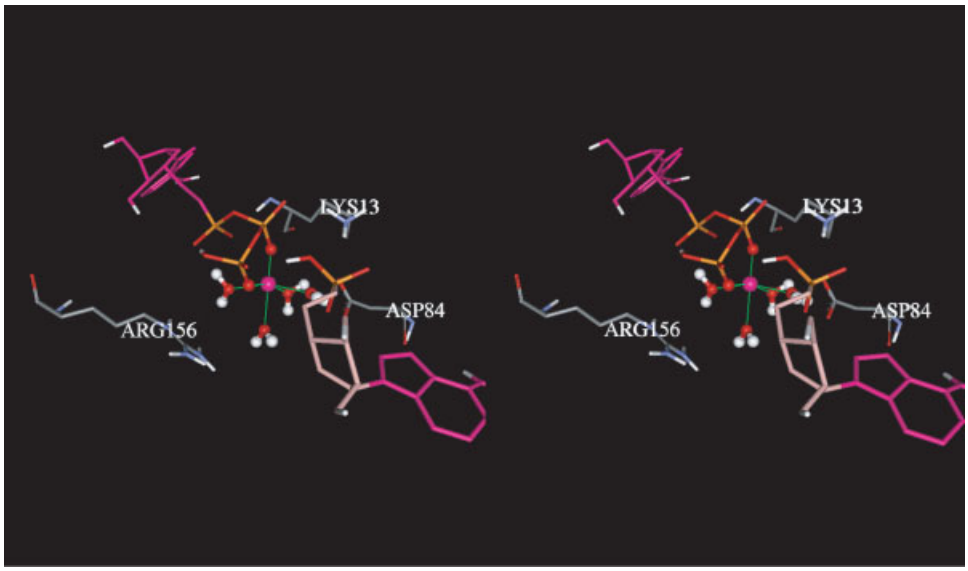

Fig. 3. The ATP-AMP-Mg^{2+}-4(H_20) complex and several of the (charged) residues that are within 7-Å radius of Mg^{2+} from a snapshot around 2.5 ns. The key catalytic residues, Lys13, Arg156, and Asp84, are displayed. Residues Ser30, Gly14, Gly12, and Gly10 are also within this radius but for clarity are not displayed.

states but, of course, also to the 1AKE* model, where AP_5A is replaced by the ATP-AMP-Mg^{2+}-4(H_20) complex. The highly charged ATP and AMP phosphate chains and Mg^{2+} can exert significant forces that extend far into the protein. Thus, differences can arise from this replacement.

The integrity of the ATP-AMP-Mg^{2+}-4(H_20) complex as the simulation proceeds is well maintained, as displayed in Figure 3. The Mg^{2+} keeps its ligation to the ATP β- and γ-PO_4 oxygens, and the 4 waters are coordinated to the Mg^{2+}, forming an octahedral coordination sphere. The distance between the ATP γ-PO_4 and AMP α-PO_4 is reasonable for a catalytically competent configuration, and residues thought to be key for catalysis are positioned close to the reactant complex, as we detail below.

The stereochemical quality of 5 snapshots of 1AKE* taken between 900 and 1500 ps was checked using the software PROCHECK v 3.5.4. The results show that 74–79% of the residues are in the most favored regions of the Ramachandran plot, and 17–23% are in the additional allowed regions (around 97% total). These numbers are comparable to values obtained from solution structures of proteins from NMR. These observations suggest that the protein does not go through disallowed dihedral conformations during the simulation.

Substrate Specificity

AMP binding site

AKs, in general, are known to have higher specificity for their nucleoside monophosphate (NMP) substrate than for their nucleoside triphosphate (NTP) substrate.[40–43] Extensive mutagenesis studies and structural data have shown that AKs control AMP specificity through several interactions with highly conserved residues.[24,44,45] The H-bonding pattern between AMP and ECAK was analyzed

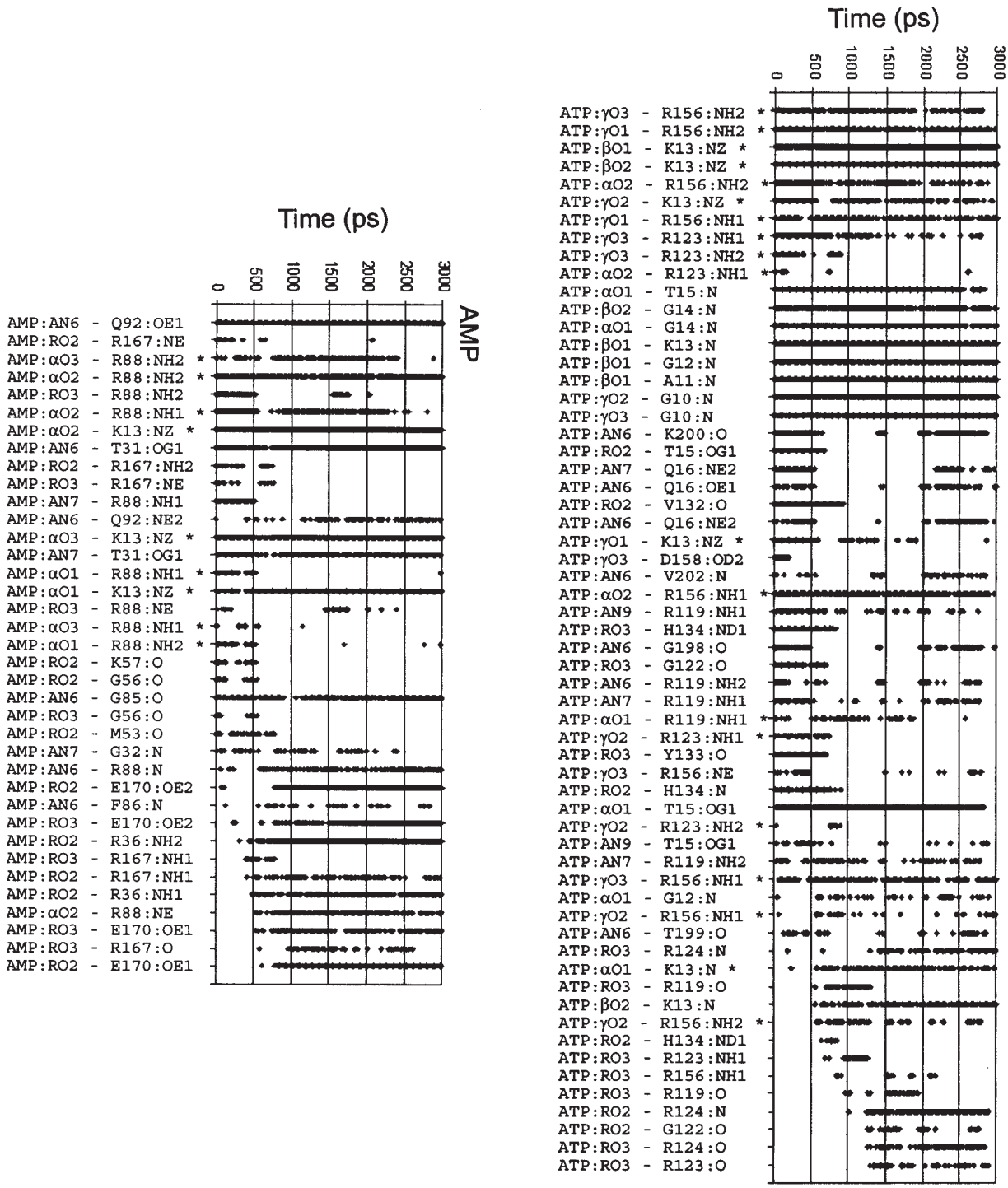

Fig. 4. H-bonds and salt bridges between the protein and ATP and between the protein and AMP during the course of the simulation. Donor and acceptor atoms within a maximum distance of 3.5 Å and a minimum angle of 120° were considered to form H-bonds. Charged donor and acceptor groups within a maximum distance of 4.5 Å were considered to form salt bridges (indicated by *). H-bond and salt bridge analyses were performed every 0.8 ps (i.e., for 3750 timepoints). Shown are only the H-bonds and salt bridges that are present at least 1.3% of the time (i.e., in at least 50 timepoints). In the designation of ATP and AMP, R denotes ribose, A denotes adenine, and α, β, and γ denote phosphates.

over the complete 3-ns simulation (Fig. 4). Figure 5 shows all the interactions of AMP and ATP with ECAK residues that are present during the 3-ns simulation.

In the 1AKE crystal structure of the ECAK · AP_5A complex,[7] AMP's adenine interacts with ECAK through 5 strong H-bonds (2 H-bonds to backbone atoms and 3

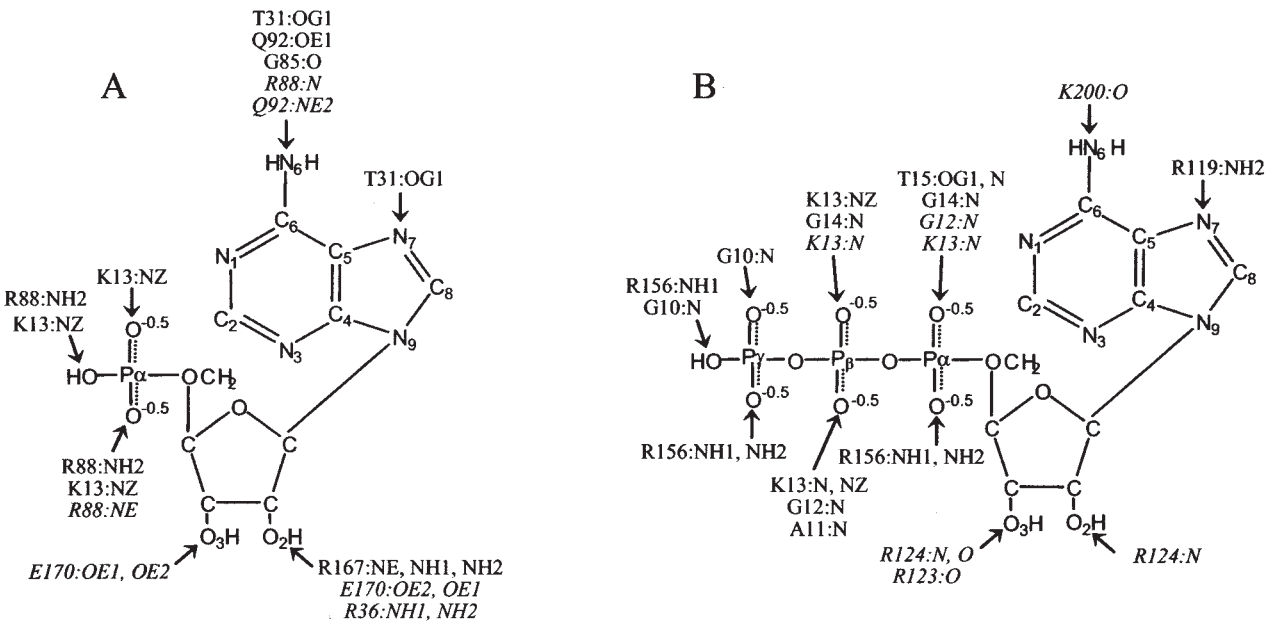

Fig. 5. Stable H-bonds and salt bridges between ECAK residues and AMP (**A**) and between ECAK residues and ATP (**B**) during the 3-ns simulation. Data were extracted from Figure 4. Regular characters: interactions present during the whole 3 ns; Italics: interactions appearing and remaining relatively stable after 500 ps or 1 ns. ATP and AMP are drawn with the −1 charge on each phosphate group split between 2 of the oxygens to indicate that the formal charge is shared.

H-bonds to side-chains) and several other less polar interactions. A strictly conserved glutamine residue, Gln92, plays a critical role both in catalysis and AMP specificity[43,44,46] through H-bonds with AMP's adenine N6. The orientation of Gln92's carboxamide is fixed by additional H-bonds to a backbone amide (from Arg88) and a conserved carboxylate (Asp61). In the simulation, plots (not shown) of the H-bonds between Asp61, Arg88, and Gln92 versus time show that Gln92's side-chain is indeed fixed by very stable H-bonds. Specifically, Gln92:NE2 H-bonds with Asp61 side-chain oxygens OD1 and OD2, and Gln 92:OE1 H-bonds with Arg 88:N. Two other H-bonds between Thr31:OG1, Gly85:O, and the adenine N6 that are stable over the trajectory also help in discriminating against guanosine monophosphate (GMP), which lacks the NH_2 group. Additionally, Thr31:OG1 forms a stable H-bond with AMP's adenine N7. Other H-bonds like adenine N6 to Phe86:N and adenine N7 to Gly32:N are on and off during the simulation (Fig. 4). Another residue, Arg88, forms transient H-bonds with the AMP adenine N6 and N7, as well as with AMP's αPO_4, and with the AMP ribose O3 (Fig. 4). These bonds are possible because Arg88's side-chain is positioned parallel to the π rings of AMP's adenine. In 1AKE,[9] Arg88 occupies 2 different conformations in the 2 molecules of the asymmetric unit. In the BSAK · AP_5A complex,[11] Arg88 adopts yet another configuration, suggesting that specific interactions between Arg88 and AMP are not what makes this residue essential in AMP binding. Arg88 is highly conserved in AKs, and its function in substrate binding and/or catalysis is the subject of ongoing discussions.

Only 1 good (2.68 Å) H-bond between AMP ribose and Lys57:O is seen in the 1AKE crystal structure. Interactions between Lys57:O and Gly56:O and the ribose are present only during the first 500 ps of the simulation (Fig. 4). However, a H-bond between the side-chain of Arg167 (involving NH1, NH2, or NE) and the ribose is present during the entire simulation (Fig. 4). In 1AKE, Arg167 is within H-bonding distance of the fourth (δ) phosphate in AP_5A. Examination of snapshots from the simulation show that the side-chain of Arg167 moves toward the ribose moiety early in the simulation. The difference in Arg167 orientation between the 1AKE crystal structure and our simulation may be due to the presence in 1AKE of the extra phosphate in AP_5A. In 1AKE, Glu170's side-chain points away from the ribose. Starting after 700 ps of our simulation, Glu170 (OE1 and OE2) forms a stable, double H-bond with AMP ribose O2 and O3 (Fig. 4). Whether this double H-bond is significant for AMP is open to question, because Glu170 is replaced by an alanine or a valine in the *B. stearothermophilus*, *Thermotoga neapolitana*, yeast, and bovine heart mitochondrial AKs.

Several arginines (Arg36, Arg88, Arg119, Arg123, Arg131, and Arg167) are situated in the active site cleft surrounding AP_5A's phosphate groups in 1AKE, presumably to help stabilize the negatively charged phosphates. Some of these arginines have been shown to participate in phosphate binding and catalysis.[7,47–50] In 1AKE, AP_5A's ϵ-PO_4 (that corresponds to AMP's α-PO_4) is well fixed through interactions with R36:NH2, R88:NH2, and R156: NH2, the latter interaction being weaker than the first two.[7] AP_5A's ϵ-PO_4 sits between the head groups of Arg88 and Arg36. Chemical modification of ECAK with phenylglyoxal completely inactivates the enzyme.[24] Reinstein et al.[24] showed that this complete inactivation is obtained by modification of a single arginine: Arg88. Mutant R88G is

1000 times less active than the wild-type ECAK, the Michaelis constant (Km) values for ATP and AMP increasing up to 5-fold and 85-fold, respectively.

The simulation results show that R88:NH2 and R88:NE have very stable interactions with AMP's α-PO_4. These interactions are salt bridge–like considering the charges of the groups involved; hence, they are much stronger than H-bonds. In a previously published 300-ps simulation of the ECAK · AP_5A complex, the interactions between Arg88 and AP_5A's ϵ-PO_4, analyzed as H-bonds, were not preserved.[29] In the 1AKE* simulation, H-bonds involving Arg36:NH1 and NH2, and Glu170:OE1 and OE2 appear after 500 ps. The Arg36 H-bonds are to the ribose, whereas in the 1AKE crystal structure, Arg36 H-bonds an ϵ-PO_4 oxygen. It seems that the removal of AP_5A's δ-PO_4 to create ATP and AMP (with the resulting loss of 2 negative charges) weakens some of the charged and polar interactions between phosphates and arginines and rearranges the H-bond and salt bridge–like interactions. The presence of Mg^{2+} can also influence the distribution of charged interactions between the protein Arg residues and the phosphate groups. Permanent H-bonds are formed between AMP's α-PO_4 and the Lys13:NZ. Lys13, situated in the P loop of all AKs, has been described as the "invariant lysine" due to dramatic loss of activity by chemical modification. In summary, interactions of Thr31, Arg88, Gly85, and Gln92 with the adenine N6 are very persistent providing the possibility of discrimination. Arg88 and Lys13 are crucial for binding the α-PO_4 and positioning it suitably to receive a phosphate group from ATP.

ATP binding site

The ATP-binding site is formed by residues in the P-loop (residues 7–15), part of the LID domain, and residues in the C-terminal helix with its connecting loop region (residues 198–214). The ATP H-bonds found in the simulation are shown in Figure 4, and the stable interactions are indicated in Figure 5. Similar to other AKs, ECAK is less specific for ATP than for AMP,[42] and most of the tight interactions between the protein and Mg-ATP involve the ATP phosphates. In the ECAK · Ap_5A complex, ATP's adenine moiety is only loosely bound to the protein through a single H-bond[7] between Lys200:O and ATP's adenine N6. This H-bond leads to a preference for ATP over guanosine triphosphate (GTP). The simulation shows (Fig. 4) that this H-bond breaks and then reforms during the 3 ns, due to fluctuations in the position of ATP's adenine. The position of Lys200 itself does not deviate much from the crystal structure, and the H-bond between Lys200:O and adenine N6 is formed whenever the adenine moiety of ATP moves to the appropriate position.

In the crystal structure, the ATP adenine is parallel to the Arg119 guanidinium group, suggesting a cation–π interaction.[7] The backbones of Pro201 and Val202 are in van der Waals contact distance of the adenine atoms. The Arg119–ATP interaction is not stable during the simulation, owing again to the large movements of ATP's adenine. N7 of the adenine ring forms an H-bond with Arg119:NH1 and NH2. Although this bond is relatively infrequent (occurring only about 8% of the time), it occurs on and off during the simulation (Fig. 4), concurrent with the movement of the adenine ring. A similar unstable H-bond is also seen between Val 202:O and ATP:AN6. Two new H-bonds between ATP:AN6 and either Tyr199:O or Gly198:O also form more or less in synchronization with the movement of the adenine ring. Taken together, none of the H-bonds are strong enough to hold ATP's adenine in place. Moreover, these interactions (with the exception of the H-bond involving Lys200) are independent of the base (it can be either adenine or guanine). While Lys200 is not conserved among the AKs, Arg119 is conserved in all known NMP kinases. These observations concur with experimental data confirming that ATP adenine is not tightly bound to the enzyme, and that it can be substituted with other NTPs such as GTP. In ECAK, the ATP adenine is quite solvent accessible, and so is Arg119; these observations probably lead to the extensive sampling of conformation space observed for ATP adenine in our MD simulation. They might also explain why the R128A mutation (equivalent to R119A in ECAK) only moderately perturbed the kinetic parameters of the chicken muscle AK1 enzyme.[28]

Only one strong H-bond between the ATP ribose O3 and Tyr133:O exists in the crystal structures of ECAK · Ap_5A and ECAK · AMP · AMPPNP. It is thought that this H-bond plays a significant role in the closing of the LID over ATP, since it is one of the few interactions between the LID and AP_5A.[2] The H-bond between Tyr133 and ribose is present only during the first 750 ps of our simulation. Even during this time, the distance between Tyr133:O and ribose:O3 is close to 3.5 Å, making it a very weak interaction and hence unlikely to be a driving force in LID closure. A weak H-bond involving His134:O and ATP's ribose O2 (at 3.48 Å in 1AKE) is present until 1000 ps. Since His134 lies in the LID domain that shows considerable backbone flexibility during the simulation (Fig. 2), this H-bond is present only during the first nanosecond. An H-bond between ATP ribose O3 and Arg124:N appears after ~1290 ps. This H-bond is fairly stable, occurring 78% of the time. Taken together, the ATP ribose, like the adenine, is also not very tightly bound to the enzyme.

In contrast to ATP ribose and adenine, the ATP phosphates have extensive contacts with the protein. The triphosphate-binding site is a highly charged pocket formed by the LID and the core. It is lined with several arginines and the P loop (glycine-rich), and it is often described as a giant anion hole.[51] Phosphate binding, orientation, and transfer are mediated by Arg36, Arg88, Arg123, Arg156, Arg167, and Lys13, all interacting with the P-loop backbone.[9] As in the case of AMP, interactions between the phosphate oxygens and the positively charged side-chains of arginines and lysines are salt bridge–like in character and hence much stronger than H-bonds.

In 1AKE, α-PO_4 shows 3 good H-bonds. It is connected in the P loop to Thr15:N (at 2.85 Å), Thr15:OG1 (at 2.71 Å), and to Gly12:N (at 2.98 Å). The α-PO_4:O2 is also within H-bonding distance from Arg123:NH2 (at 2.91 Å). Thr23 (Thr15 in ECAK) in chicken muscle AK1 displays strong

nuclear Overhauser effects (NOEs) with the adenosine moiety of Mg-ATP,[52] although it is within H-bonding distance from the ATP α-PO_4 in the AK1 crystal structure. Phosphate stereochemistry experiments in AK1 also suggest that Thr23 directly interacts with α-PO_4.[53] This result agrees with the 1AKE structure, in which Thr15:OG1 forms 2 stable H-bonds with α-PO_4. Based on these observations, it was suggested that in AK1, Thr23 plays a role in catalysis through direct interaction with ATP.[53] Although Thr23 is conserved in all known AKs, the mild perturbations of mutant T23A's kinetic parameters (k_{cat} and K_m) are insufficient to confirm a functional role for Thr23.[53] In our simulation, Thr15:OG1 and Thr15:N form permanent H-bonds with α-PO_4 (Figs. 4 and 5) in accord with its suggested catalytic role. Thr15 also forms transitory H-bonds with ATP adenine N6, N7, and N9, in keeping with its proximity to ATP adenine, as seen in the solution structure of AK1 and in the crystal structure of the yeast AK · Mg-Ap_5A complex.[13] These H-bonds are weaker, lasting for at most 500 ps.

The H-bond between Gly12:N and ATP's α-PO_4 seen in the 1AKE structure is present only rarely during the simulation. The on–off nature of this H-bond in the simulation originates from fluctuations in the position of the phosphate relative to Gly12. Instead, we observe a stable H-bond between ATP α-PO_4 and Gly14:N throughout the simulation. The salt bridge–like interaction with Arg123:NH1 is present only for 100 ps, with the side-chain of Arg123 moving away from ATP early in the simulation. The ATP phosphate chain adopts a slightly different position in the equilibrated 1AKE* compared to that in 1AKE. α-PO_4 is farther away from Arg123 in 1AKE* than in 1AKE, leading to a weaker salt bridge–like interaction. The side-chain of Arg123 is thus able to fluctuate and move away from α-PO_4 during the simulation. This side-chain, however, moves within 4.5 Å of ATP γ-PO_4, thus creating another potential salt bridge interaction. Note that in the 1AKE crystal structure, Arg123:NH1 is 3.94 Å from a γ-PO_4 oxygen providing a bifurcated situation that, when the extra AP_5A PO_4 is removed, most likely leads to the observed repositioning of Arg123 in the simulation. In our simulation, the charge compensation for α-PO_4 is provided by its salt bridge interaction with Arg156:NH1, which is present about 50% of the time (Fig. 4), rather than its salt bridge with Arg123:NH1. Another H-bond not found in 1AKE forms between ATP α-PO_4 and Lys13:N after 600 ps, and it is present during most of the remaining 2.4 ns. Arg119:NH1 is within 4.5 Å of α-PO_4 until about 1750 ps. Even during this time, the interaction is weak and intermittent.

In 1AKE, β-PO_4 is very well connected to the P loop through as many as 4 strong H-bonds with Ala11:N, Gly12:N, Lys13:N, and Gly14:N, and through a salt bridge with Lys13:NZ. Almost all the H-bonds involving ATP β-PO_4 have a strong presence throughout the simulation (Fig. 4). The invariant P-loop lysine, Lys13, forms a permanent H-bond with Ala8:O during the simulation (not shown), thus acting as a bridge between Ala8 and ATP phosphate chain. The stability of this H-bond underlines the importance of the bridge in maintaining the integrity of the P-loop, since Ala8 and Lys13 are at opposite ends of the P-loop. Another H-bond between Lys13:NZ and Gly7:O is also present throughout the simulation, confirming the structural importance of Lys13. At no point is there an H-bond between the side-chain of Arg123 and β-PO_4 as seen in 1AKE. With a donor–acceptor distance of 3.3 Å in 1AKE, the H-bond between Arg123:NH2 and β-PO_4 is weak even in the crystal structure.

The to-be-transferred γ-PO_4 is loosely bound, with fewer interactions with the active site residues than α-PO_4 and β-PO_4 in 1AKE, only forming salt bridge–like interactions with Lys13:NZ and Arg123:NH2, and weakly interacting with Arg156:NH2. In the BSAK · Mg-Ap_5A complex, γ-PO_4 is within H-bonding distance of Lys13, and within 4.5 Å of the side-chains of Arg123 (NH1 and NH2) and Arg156. These H-bonds have donor–acceptor distances of 3.3 Å or more, indicating weaker interactions with the protein as compared to ATP's α-PO_4 and β-PO_4. In our simulation, the salt-bridges between γ-PO_4 and Arg156:NH1 and NH2 are present as in the crystal structure. The interactions with Lys13 and Arg123 are not stable in the simulation. They are replaced by other interactions arising from the presence of Mg^{2+}, and from the enhanced conformational range available to γ-PO_4, which is no longer covalently attached to AP_5A's δ-PO_4. γ-PO_4 is now free to rotate and, with its negative charges, it strongly interacts with Mg^{2+}. An additional H-bond not seen in the crystal structures is seen in our simulation between Gly10:N and γ-PO_4. This H-bond is stable throughout the simulation and it is the only link between γ-PO_4 and the P loop.

In summary, we see about the same interactions between the ATP phosphate chain and the P loop (main-chain and side-chains) as in the crystal structure, but we see more and stronger interactions with Arg156 than with Arg123, for both β-PO_4 and γ-PO_4. Without exception, all permanent H-bonds between ATP and the protein in 1AKE* in the simulation involve the 3 ATP phosphate groups (Figs. 4 and 5), the ATP adenine and ribose moieties being only loosely bound to the protein.

Role and conformation of active site residues around Mg^{2+}

Kinases require a divalent cation, usually Mg^{2+}, for catalysis. The ATP β- and γ-phosphates are coordinated to Mg^{2+}, and the true substrate for AKs is Mg^{2+}-ATP. Mg^{2+} serves to neutralize the highly negative charge on the ATP triphosphate, thereby reducing electrostatic repulsion of the transferred phosphate and increasing the efficiency of nucleophilic attack. In AKs, conserved serine, threonine, or aspartate residues participate in binding the Mg^{2+} cation, coordinating it either directly in the first coordination sphere or indirectly through water molecules.

In porcine muscle AK · CoATP, AK · CoGTP, and AK · CoGDP, ^{31}P NMR relaxation rates indicate that Co^{2+} is directly coordinated to only β-PO_4 (GDP) or β-PO_4 and γ-PO_4 (ATP and GTP).[54] In addition, α-PO_4 is too far from Co^{2+} to be in the first coordination sphere, but also too close to be in the second coordination sphere (not enough

room for a water molecule). These results suggest that ATP-Mg^{2+} binds AK as a β,γ bidentate complex rather than an α,β,γ tridentate complex. In the structure of the BSAK · Mg^{2+}-AP_5A complex, Mg^{2+} is coordinated to the phosphates corresponding to ATP's β- and γ-phosphates, and to 4 water molecules numbered 300–303.[11] Mg^{2+}-AP_5A is anchored to BSAK through several H-bond networks mediated by the 4 Mg^{2+}-coordinating water molecules. Waters 300 and 303 help orient the α-PO_4 of AMP. Water 300 is also positioned to interact with Arg36 and Asp33, thus linking Mg^{2+}-AP_5A to the protein. Water 302 is within H-bond distance of ATP's 3 phosphate groups, reinforcing the linkage between the phosphate chain and Mg^{2+}. Water 301 H-bonds to Asp84:OD2 and Gly14:N, and it is the only water that does not interact with the phosphates. It is evident that this H-bond network is important for orienting the donor and acceptor phosphates and aiding the ternary complex to proceed to the transition state. Based on their 300-ps simulation results of ECAK · AP_5A, Kern et al. predicted that 3 aspartate residues, Asp84, Asp33, and Asp110, are possible candidates for binding the Mg^{2+} complex.[29] Ser30, Thr31, and Thr89 were also suitably placed and were available to interact with Mg^{2+}. Orientation of the side-chains of these residues and the position of the phosphate chain left just enough room for the Mg^{2+} ion.

In the simulation, Mg^{2+} remains coordinated to 4 waters (218–221) as dictated by the force field (see the Methods section). The water–Mg^{2+} distances are short in the crystal structure, indicating that these waters are ligated to the ion. Then, one can choose to modify the force field by inserting specific "covalent" bonds, or by using noncovalent but relatively strong interactions,[55] as we have done. Even though no such interactions were introduced between Mg^{2+} and ATP β- and γ-phosphates, we find that throughout the simulation Mg^{2+} is also coordinated to ATP's β-PO_4 through its O2 oxygen, and to ATP's γ-PO_4 through its O1 oxygen. As shown in Figure 6, the coordination is close to octahedral. Furthermore, the additional flexibility introduced by having ATP/AMP versus AP_5A in the structure, as in the 1ZIO crystal structure, still preserves the octahedral geometry.

A second coordination sphere for Mg^{2+} includes Asp84:OD1 and OD2 that have waters 219 and 221 (equivalent to waters 301 and 303 in BSAK) screening this direct salt bridge–like interaction. The H-bonds between water molecules 219 and 221 and the side-chain of Asp84 are very stable over the 3-ns trajectory (not shown), indicating the importance of Asp84 in binding the Mg^{2+}–water complex. In AK1, mutation of the corresponding Asp93 to alanine decreased the k_{cat} 650-fold.[56] The D93A mutant showed no structural perturbation as evidenced by NMR analysis, indicating a local effect. Moreover, the AK1 D93A mutant had a markedly lower affinity for Mg^{2+}.[56] Similar effects were also observed for the ECAK D84A mutant.[26] Considering the fact that Mg^{2+} plays a dual structural and chemical role in catalysis, these results suggest that Asp84 is important in the structural role of Mg^{2+}. Specifically, in the AK1 D93A mutant, Mg^{2+} may be unable to orient the phosphate chain for the transfer.[56]

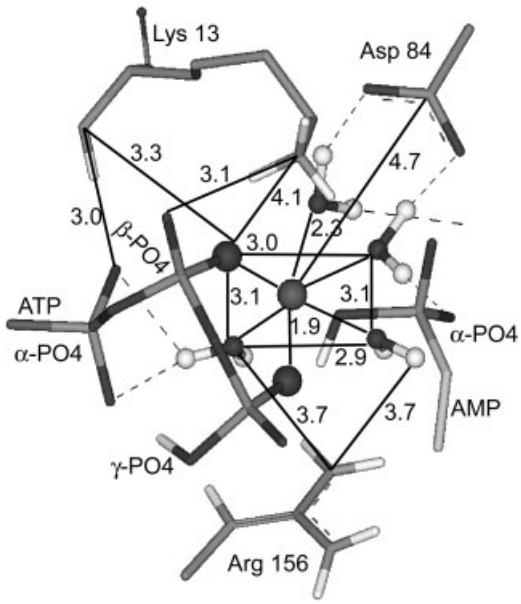

Fig. 6. Mg^{2+} coordination sphere. The 4 Mg^{2+}-coordinated waters, the β-PO_4:O2, and the γ-PO_4:O1 form an essentially octahedral first coordination sphere. The multifunctional role of Lys13 in anchoring ATP and AMP is evident. Asp84 is in the second coordination sphere and is H-bonded to 2 of the Mg^{2+}-coordinated waters. Arg156 is almost in H-bonding distance of the other two Mg^{2+}-coordinated waters and may be positioned to participate in catalysis. See text for further discussion. Distances are in angstroms.

Throughout the simulation, Asp84's main- and side-chains form a stable network of H-bonds. Besides the above-mentioned H-bonds with waters 219 and 221, Asp84 forms stable H-bonds with Ser30 and Thr31. The H-bond between Asp84 and Thr31 backbone atoms is particularly significant, since Thr31 is also stably linked to AMP's adenine. Thus, these interactions anchor AMP to the Mg^{2+} complex involving the ATP phosphate chain. Asp84 interacts with Ser30 and Ile29 through strong H-bonds and also forms a persistent salt bridge with Lys13:NZ in the P-loop. Additionally, Ser30 is by itself coordinated to the Mg^{2+} ion through water molecule 219.

As in BSAK, water molecule 220 (water 302 in 1ZIO), is within H-bonding distance of ATP α-, β-, and γ-phosphates, strengthening the Mg^{2+}–phosphate complex and properly orienting the ATP phosphate chain. Interactions not seen in BSAK but transiently present in the 1AKE* simulation include H-bonds between Arg156 and waters 220 and 218. Arg156 has been implicated in the stabilization of the transition state. Another rather weak H-bond is also seen between Gly14:N and water molecule 219. A corresponding H-bond is present in 1ZIO involving Gly14 and water molecule 301.

Lysine, with its backbone amide, long and flexible side-chain, and charged head group, is well-suited for a multifunctional role. These features are apparent in Figure 6, where Lys13 stabilizes the active site by forming H-bonds and salt bridge–like interactions with both ATP and AMP using its flexibility and multifunctionality. The

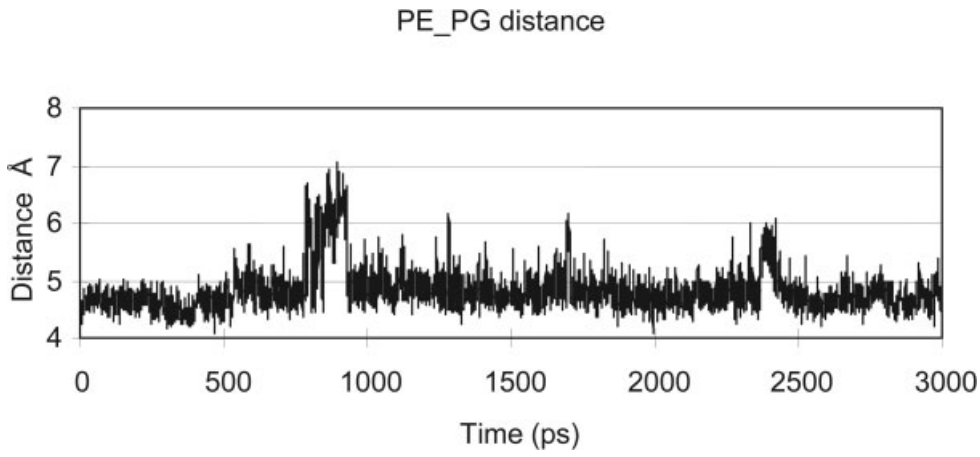

Fig. 7. Distance between the ATP γ-P and AMP α-P atoms during the 3-ns simulation.

other interactions of Lys13 are discussed in previous sections.

Catalytic Mechanism

The 1AKE* simulation can be used to suggest whether the mechanism of phosphoryl transfer is associative or dissociative, at least from the perspective of geometrical requirements. The consensus is that in enzymes in general,[31–34,57] and in AKs in particular,[25,43] an associative mechanism is operative. The geometric criterion for an associative mechanism is that the transition state has sufficiently short entering and leaving group distances to support reasonably large fractional bond numbers, n. For example, if an S_N2 mechanism were operative ($n = \frac{1}{2}$) the P–O distance would be 1.91 Å, while if a fully associative mechanism were operative ($n = 1$), the P–O distance would be 1.73 Å, the P–O single-bond distance.

In Figure 7, the ATP γ–P to AMP α–P distance is plotted during the 3-ns simulation time. For most of the time, this distance ranges between 4.5 Å and 5.0 Å, about 1 Å greater than the 3.8-Å van der Waals P–P contact distance. In the absence of the Mg^{2+} cation and Lys13, with its ability to span ATP and AMP, it would be difficult to support the close approach of these (negatively charged) phosphate groups. The P–P distance suggests that an associative mechanism could be operative in AKE, as illustrated in Figure 8. The atoms ATP β–P, Lys13:NZ and AMP α–P form an essentially equilateral triangle with apex Lys13:NZ and equal legs ATP β-P–Lys13:NZ and Lys13:NZ–AMP α-P. The atoms Lys13:NZ, ATP β–P, ATP γ–P, and AMP α–P form a plane, where the ATP β-P–AMP α-P distance is approximately twice that of the ATP β-P–ATP γ-P distance. Thus, there would be room to rotate the ATP γ-PO_4 into a line formed by ATP β–P, ATP γ–P, and AMP α–P and produce a trigonal bipyrimidal phosphorane transition state, as suggested by Reinstein et al.[25] In this configuration, Lys13:NZ would be positioned above the 3 apical oxygens, those in the plane perpendicular to the ATP β–P, ATP γ–P, and AMP α–P line. The Mg^{2+} ($4H_2O$) complex is below the above-mentioned plane, with Mg^{2+} equidistant from the oxygens (shown as spheres) associated with ATP β–P and ATP γ–P. From these geometrical considerations, the role played by Mg^{2+} ($4H_2O$) and Lys13 in maintaining the proximity and orientation of the ATP and AMP phosphates appropriate for phosphoryl transfer is clarified.

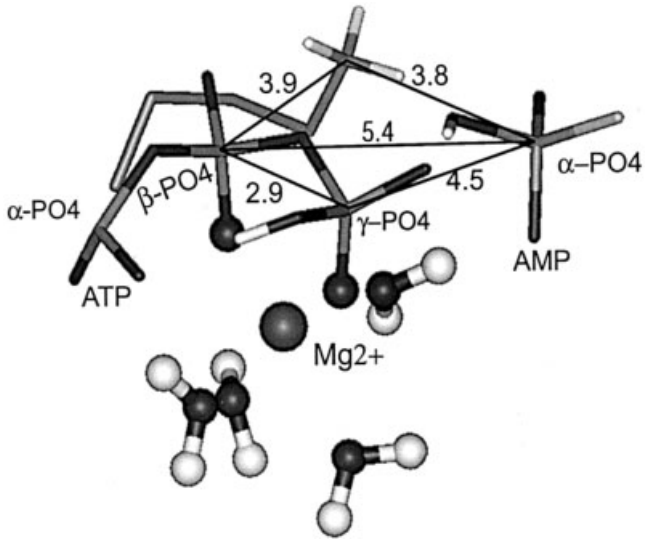

Fig. 8. Geometry of Mg^{2+} association with its 4 coordinating waters, ATP and AMP phosphates, and Lys13. The displayed geometry has room for the ATP γ-PO_4 to rotate and line up the ATP β-P, ATP γ-P, and AMP α-P, and to produce a trigonal bipyrimidal phosphorane transition state. Distances are in angstroms.

CONCLUSIONS

MD simulation of the ECAK · Mg–ATP · AMP ternary reactant complex that we constructed shows general agreement with conclusions drawn from the analysis of the crystallographic and other studies of ECAK complexed with AP_5A. The strong repulsive interaction between the terminal, negative phosphate groups that results from the split of AP_5A into ATP and AMP is counteracted by the presence of Mg^{2+} and, presumably, some of the positively charged surrounding residues. The AMP adenine N6 strongly interacts with the protein through H-bonds, which

forms the basis for NMP specificity. In contrast, and also in agreement with conclusions drawn from the crystallographic data,[6] the ATP adenine and ribose moieties are only loosely bound to the protein, while the phosphates interact strongly with nearby residues.

Octahedral coordination of the Mg^{2+} by 4 waters and by oxygens of ATP β- and γ-phosphates is maintained throughout the simulation. The conserved Lys13 in the P loop bridges the ATP and AMP phosphates, a phenomenon that relies on the lysine side-chain's unique properties of flexibility and H-bond–salt bridge capability. In addition to Lys13, the Mg^{2+}, its coordination waters, and some surrounding charged residues maintain the AMP α-phosphate and ATP β- and γ-phosphates in a configuration suggesting that phosphoryl transfer occurs by an associative mechanism in AK.

The simulation results could provide a starting point for a combined quantum mechanical–molecular mechanical simulation of the reaction mechanism for phosphoryl transfer.

REFERENCES

1. Walsh C. Enzymatic reaction mechanisms. San Francisco: W. H. Freeman; 1979. 978 p.
2. Schulz GE, Muller CW, Diederichs K. Induced-fit movements in adenylate kinases. J Mol Biol 1990;213:627–630.
3. Schulz GE. Induced-fit movements in adenylate kinases. Faraday Discuss 1992;93:85–93.
4. Vieille C, Krishnamurthy H, Hyun HH, Savchenko A, Yan H, Zeikus JG. *Thermotoga neapolitana* adenylate kinase is highly active at 30°C. Biochem J 2003;372:577–585.
5. Dreusicke D, Karplus PA, Schulz GE. Refined structure of porcine cytosolic adenylate kinase at 2.1 Å resolution. J Mol Biol 1988;199: 359–371.
6. Müller CW, Schulz GE. Structure of the complex of adenylate kinase from *Escherichia coli* with the inhibitor P1,P5-di(adenosine-5′-)pentaphosphate. J Mol Biol 1988;202:909–912.
7. Müller CW, Schulz GE. Structure of the complex between adenylate kinase from *Escherichia coli* and the inhibitor Ap5A refined at 1.9 Å resolution: a model for a catalytic transition state. J Mol Biol 1992;224:159–177.
8. Müller CW, Schulz GE. Crystal structures of two mutants of adenylate kinase from *Escherichia coli* that modify the Gly-loop. Proteins 1993;15:42–49.
9. Berry MB, Meador B, Bilderback T, Liang P, Glaser M, Phillips GN Jr. The closed conformation of a highly flexible protein: the structure of *E. coli* adenylate kinase with bound AMP and AMPPNP. Proteins 1994;19:183–198.
10. Müller CW, Schlauderer GJ, Reinstein J, Schulz GE. Adenylate kinase motions during catalysis: an energetic counterweight balancing substrate binding. Structure 1996;4:147–156.
11. Berry MB, Phillips GNJ. Crystal structures of *Bacillus stearothermophilus* adenylate kinase with bound Ap_5A, Mg^{2+} Ap_5A, and Mn^{2+} Ap_5A reveal an intermediate LID position and six coordinate octahedral geometry for bound Mg^{2+} and Mn^{2+}. Proteins 1998;32:276–288.
12. Abele U, Schulz GE. High-resolution structures of adenylate kinase from yeast ligated with inhibitor Ap_5A, showing the pathway of phosphoryl transfer. Protein Sci 1995;4:1262–1271.
13. Egner U, Tomasselli AG, Schulz GE. Structure of the complex of yeast adenylate kinase with the inhibitor P1,P5-di(adenosine-5′-)pentaphosphate at 2.6 Å resolution. J Mol Biol 1987;195:649–658.
14. Diederichs K, Schulz GE. Three-dimensional structure of the complex between the mitochondrial matrix adenylate kinase and its substrate AMP. Biochemistry 1990;29:8138–8144.
15. Schlauderer GJ, Proba K, Schulz GE. Structure of a mutant adenylate kinase ligated with an ATP-analogue showing domain closure over ATP. J Mol Biol 1996;256:223–227.
16. Schlauderer GJ, Schulz GE. The structure of bovine mitochondrial adenylate kinase: Comparison with isoenzymes in other compartments. Protein Sci 1996;5:434–441.
17. Sheng XR, Li X, Pan XM. An iso-random Bi Bi mechanism for adenylate kinase. J Biol Chem 1999;274:22238–22242.
18. Sinev MA, Sineva EV, Ittah V, Haas E. Domain closure in adenylate kinase. Biochemistry 1996;35:6425–6437.
19. Lin Y, Nageswara Rao BD. Structural characterization of adenine nucleotides bound to *Escherichia coli* adenylate kinase: 1. Adenosine conformations by proton two-dimensional transferred nuclear Overhauser effect spectroscopy. Biochemistry 2000;39:3636–3646.
20. Lin Y, Nageswara Rao BD. Structural characterization of adenine nucleotides bound to *Escherichia coli* adenylate kinase: 2. ^{31}P and ^{13}C relaxation measurements in the presence of cobalt(II) and manganese(II). Biochemistry 2000;39:3647–3655.
21. Shapiro YE, Sinev MA, Sineva EV, Tugarinov V, Meirovitch E. Backbone dynamics of *Escherichia coli* adenylate kinase at the extreme stages of the catalytic cycle studied by (15)N NMR relaxation. Biochemistry 2000;39:6634–6644.
22. Shapiro YE, Kahana E, Tugarinov V, Liang ZC, Freed JH, Meirovitch E. Domain flexibility in ligand-free and inhibitor-bound *Escherichia coli* adenylate kinase based on a mode-coupling analysis of N-15 spin relaxation. Biochemistry 2002;41:6271–6281.
23. Reinstein J, Brune M, Wittinghofer A. Mutations in the nucleotide binding loop of adenylate kinase of *Escherichia coli*. Biochemistry 1988;27:4712–4720.
24. Reinstein J, Gilles AM, Rose T, Wittinghofer A, Saint Girons I, Barzu O, Surewicz WK, Mantsch HH. Structural and catalytic role of arginine 88 in *Escherichia coli* adenylate kinase as evidenced by chemical modification and site-directed mutagenesis. J Biol Chem 1989;264:8107–8112.
25. Reinstein J, Schlichting I, Wittinghofer A. Structurally and catalytically important residues in the phosphate binding loop of adenylate kinase of *Escherichia coli*. Biochemistry 1990;29:7451–7459.
26. Rose T, Glaser P, Surewicz WK, Mantsch HH, Reinstein J, Le Blay K, Gilles AM, Barzu O. Structural and functional consequences of amino acid substitutions in the second conserved loop of *Escherichia coli* adenylate kinase. J Biol Chem 1991;266:23654–23659.
27. Rose T, Brune M, Wittinghofer A, Le Blay K, Surewicz WK, Mantsch HH, Barzu O, Gilles AM. Structural and catalytic properties of a deletion derivative (Δ133–157) of *Escherichia coli* adenylate kinase. J Biol Chem 1991;266:10781–10786.
28. Tsai MD, Yan HG. Mechanism of adenylate kinase: site-directed mutagenesis versus X-ray and NMR. Biochemistry 1991;30:6806–6818.
29. Kern P, Brunne RM, Folkers G. Nucleotide-binding properties of adenylate kinase from *Escherichia coli*: a molecular dynamics study in aqueous and vacuum environments. J Comput Aided Mol Des 1994;8:367–838.
30. Elamrani S, Berry MB, Phillips GN, McCammon JA. Study of global motions in proteins by weighted masses molecular dynamics: adenylate kinase as a test case. Proteins 1996;25:79–88.
31. Knowles JR. Enzyme-catalyzed phosphoryl transfer reactions. Ann Rev Biochem 1980;49:877–919.
32. Hollfelder F, Herschlag D. The nature of the transition-state for enzyme-catalyzed phosphoryl transfer—hydrolysis of O-aryl phosphorothioates by alkaline-phosphatase. Biochemistry 1995;34: 12255–12264.
33. Matte A, Tari LW, Delbaere LTJ. How do kinases transfer phosphoryl groups? Structure 1998;6:413–419.
34. Lahiri SD, Zhang GF, Dunaway-Mariano D, Allen KN. The pentacovalent phosphorus intermediate of a phosphoryl transfer reaction. Science 2003;299:2067–2071.
35. van Gunsteren WF, Billeter SR, Eising AA, Hünnenberger PH, Krüger P, Mark AE, Scott WRP, Tironi IG. Biomolecular simulation: the GROMOS96 manual and user guide. Zürich: Vdf Hochschulverlag AG an der ETH Zürich; 1996.
36. Tsodikov OV, Record MTJ, Sergeev YV. A novel computer program for fast exact calculation of accessible and molecular surface areas and average surface curvature. J Comput Chem 2002;23: 600–609.
37. Cukier RI, Seibold SA. Molecular dynamics simulations of prostaglandin endoperoxide II synthase-1: role of water and the mechanism of compound I formation from hydrogen peroxide. J Phys Chem B 2002;106:12031–12044.

38. Hockney RW, Eastwood JW. Computer simulation using particles. New York: McGraw-Hill; 1981. 540 p.
39. Allen MP, Tildesley DJ. Computer simulation of liquids. Oxford, UK: Clarendon Press; 1987. 385 p.
40. Tomasselli AG, Noda LH. Mitochondrial ATP:AMP phosphotransferase from beef heart: purification and properties. Eur J Biochem 1980;103:481–491.
41. Ito Y, Tomasselli AG, Noda LH. ATP:AMP phosphotransferase from baker's yeast: purification and properties. Eur J Biochem 1980;105:85–92.
42. Saint Girons I, Gilles AM, Margarita D, Michelson S, Monnot M, Fermandjian S, Danchin A, Barzu O. Structural and catalytic characteristics of *Escherichia coli* adenylate kinase. J Biol Chem 1987;262:622–629.
43. Yan H, Tsai MD. Nucleoside monophosphate kinases: structure, mechanism, and substrate specificity. Adv Enzymol Relat Areas Mol Biol 1999;73:103–134.
44. Beichner S, Byeon I-JL, Tsai M-D. Structure–function relationship of adenylate kinase: Glu-101 in AMP specificity. In: Kaumaya PTP, Hodges RS, editors. Peptides: chemistry, structure and biology. Kingswinford, UK: Mayflower Scientific; 1996. p 721–723.
45. Okajima T, Tanizawa K, Yoneya T, Fukui T. Role of leucine 66 in the asymmetric recognition of substrates in chicken muscle adenylate kinase. J Biol Chem 1991;266:11442–11447.
46. Okajima T, Tanizawa K, Fukui T. Site-directed random mutagenesis of AMP-binding residues in adenylate kinase. J Biochem 1993;114:627–633.
47. Kim HJ, Nishikawa S, Tokutomi Y, Takenaka H, Hamada M, Kuby SA, Uesugi S. In vitro mutagenesis studies at the arginine residues of adenylate kinase: a revised binding site for AMP in the X-ray-deduced model. Biochemistry 1990;29:1107–1111.
48. Yan HG, Dahnke T, Zhou BB, Nakazawa A, Tsai MD. Mechanism of adenylate kinase: critical evaluation of the X-ray model and assignment of the AMP site. Biochemistry 1990;29:10956–10964.
49. Yan HG, Shi ZT, Tsai MD. Mechanism of adenylate kinase: structural and functional demonstration of arginine-138 as a key catalytic residue that cannot be replaced by lysine. Biochemistry 1990;29:6385–6392.
50. Dahnke T, Shi Z, Yan H, Jiang RT, Tsai MD. Mechanism of adenylate kinase: structural and functional roles of the conserved arginine-97 and arginine-132. Biochemistry 1992;31:6318–6328.
51. Dreusicke D, Schulz GE. The glycine-rich loop of adenylate kinase forms a giant anion hole. FEBS Lett 1986;208:301–304.
52. Byeon IJ, Yan H, Edison AS, Mooberry ES, Abildgaard F, Markley JL, Tsai MD. Mechanism of adenylate kinase: 1H, 13C, and 15N NMR assignments, secondary structures, and substrate binding sites. Biochemistry 1993;32:12508–12521.
53. Shi Z, Byeon IJ, Jiang RT, Tsai MD. Mechanism of adenylate kinase: What can be learned from a mutant enzyme with minor perturbation in kinetic parameters? Biochemistry 1993;32:6450–6458.
54. Ray BD, Rosch P, Rao BD. ^{31}P NMR studies of the structure of cation-nucleotide complexes bound to porcine muscle adenylate kinase. Biochemistry 1988;27:8669–8676.
55. Banci L. Molecular dynamics simulations of metalloproteins. Curr Opin Chem Biol 2003;7:143–149.
56. Yan HG, Tsai MD. Mechanism of adenylate kinase: demonstration of a functional relationship between aspartate 93 and Mg^{2+} by site-directed mutagenesis and proton, phosphorus-31, and magnesium-25 NMR. Biochemistry 1991;30:5539–5546.
57. Mildvan AS. Mechanisms of signaling and related enzymes. Proteins 1997;29:401–416.